Hexokinase 2 displacement from mitochondria-associated membranes prompts Ca^{2+}-dependent death of cancer cells

Francesco Ciscato[1], Riccardo Filadi[1], Ionica Masgras[1], Marco Pizzi[2], Oriano Marin[1], Nunzio Damiano[1], Paola Pizzo[1], Alessandro Gori[3], Federica Frezzato[4], Federica Chiara[5], Livio Trentin[4], Paolo Bernardi[1] (iD) & Andrea Rasola[1,*] (iD)

Abstract

Cancer cells undergo changes in metabolic and survival pathways that increase their malignancy. Isoform 2 of the glycolytic enzyme hexokinase (HK2) enhances both glucose metabolism and resistance to death stimuli in many neoplastic cell types. Here, we observe that HK2 locates at mitochondria-endoplasmic reticulum (ER) contact sites called MAMs (mitochondria-associated membranes). HK2 displacement from MAMs with a selective peptide triggers mitochondrial Ca^{2+} overload caused by Ca^{2+} release from ER via inositol-3-phosphate receptors (IP3Rs) and by Ca^{2+} entry through plasma membrane. This results in Ca^{2+}-dependent calpain activation, mitochondrial depolarization and cell death. The HK2-targeting peptide causes massive death of chronic lymphocytic leukemia B cells freshly isolated from patients, and an actionable form of the peptide reduces growth of breast and colon cancer cells allografted in mice without noxious effects on healthy tissues. These results identify a signaling pathway primed by HK2 displacement from MAMs that can be activated as anti-neoplastic strategy.

Introduction

Hexokinases are a family of four isoforms that catalyze phosphorylation of glucose, making it available for utilization in glycolysis, pentose phosphate pathway, glycogenesis, and hexosamine biosynthesis [1].

HK2, the most active isozyme, is markedly expressed in cells characterized by a high rate of glucose consumption, such as adipose, skeletal, and cardiac muscle. During the neoplastic process, metabolic changes are required to allow cell growth in conditions of fluctuating nutrient and oxygen availability [2]. HK2 plays a major role in this metabolic rewiring [3–5], being induced by oncogenic K-Ras activation [6] or in response to (pseudo)hypoxia [7,8]. HK2 is mainly bound to the outer mitochondrial membrane, where it can gain privileged access to newly synthesized ATP, thus increasing efficiency in glucose usage [9], while following glucose deprivation HK2 elicits autophagy by inhibiting mTORC1 [10]. HK2 binding to mitochondria is increased by Akt phosphorylation, a key metabolic event occurring downstream to many signaling pathways hyperactivated in tumor cells [11], and by interactions with DMPK and Src kinases [12], whereas it is inhibited by the Akt-antagonizing phosphatase PHLPP and by hexokinase enzymatic product glucose-6-phosphate [10]. Moreover, mitochondrial HK2 takes part in the protection of cancer cells from noxious stimuli through poorly defined mechanisms that include antagonizing the activity of pro-apoptotic Bcl-2 family proteins and increasing anti-oxidant defenses through interaction with the fructose-2,6-bisphosphatase TIGAR, which elicits pentose phosphate pathway induction [13]. In cancer patients, HK2 induction is related to stage progression, acquisition of invasive and metastatic capabilities, and poor prognosis [14]. HK2 promotes neoplastic growth in glioblastoma multiforme [15], confers chemoresistance in epithelial ovarian cancer [16], and is required for tumor onset and maintenance in mouse models of lung and breast cancer, where its genetic ablation is therapeutic without adverse effects [6].

Thus, HK2 constitutes a promising target for developing anti-neoplastic strategies, but the clinical use of hexokinase inhibitors is hampered by lack of specificity or side effects [17] potentially associated with glucose metabolism derangement. A possible alternative approach is detaching HK2 from mitochondria, as we and others have previously shown that this can induce opening of a mitochondrial

1 Department of Biomedical Sciences (DSB), University of Padova, Padova, Italy
2 Surgical Pathology and Cytopathology Unit, Department of Medicine (DIMED), University of Padova, Padova, Italy
3 CNR Institute of Chemistry of Molecular Recognition (ICRM), Milano, Italy
4 Hematology and Clinical Immunology Branch, Department of Medicine (DIMED), University of Padova, Padova, Italy
5 Department of Surgery, Oncology and Gastroenterology (DISCOG), University of Padova, Padova, Italy
  *Corresponding author. Tel: +39 049 8276062; E-mail: andrea.rasola@unipd.it

channel, the permeability transition pore (PTP), and consequently cell death [12,13,18,19]. However, both a detailed comprehension of the molecular mechanisms leading to cell damage and the development of a HK2-targeting tool that is operational in *in vivo* tumor models are required to translate this information into the groundwork for future anti-neoplastic approaches.

Here, we demonstrate that in neoplastic cells, HK2 localizes in MAMs, specific subdomains of interaction between mitochondria and ER. HK2 detachment from MAMs rapidly elicits a massive Ca^{2+} flux into mitochondria and consequently a calpain-dependent cell death. We ignite this process with a HK2-targeting peptide composed by modular units that can be adapted to *in vivo* delivery, without affecting hexokinase enzymatic activity and with no adverse effects on animal models.

Results and Discussion

HK2 localizes in MAMs of neoplastic cells

Dissection of submitochondrial HK2 localization can provide important functional clues, as mitochondria compartmentalize specific activities in domains formed by multiprotein platforms. After confirming that HK2 associates with tumor cell mitochondria (Fig 1A), we have found that it specifically localizes in MAMs by merging the fluorescence of HK2-conjugated antibodies with mitochondria-targeted YFP and ER-targeted CFP (Fig 1B) or with a split-GFP-based probe for ER-mitochondria contacts (SPLICS$_L$) [20] (Fig 1C). These experiments have been extended to diverse HK2-expressing tumor cell models (Fig EV1A and B), and their quantification indicate both that 70–80% of HK2 localizes in MAMs and that most cellular MAMs harbor HK2 proteins (Fig 1D–F). Interestingly, the use of a short-range, split-GFP-based approach (SPLICS$_S$) [20] designed to identify proteins localized in the tighter MAM fraction does not detect HK2 (Fig EV1C). The SPLICS$_L$ analysis also showed that HK2 is significantly enriched in MAMs with respect to TOM20, a protein that is uniformly distributed in the outer mitochondrial membrane (Fig EV1D). MAMs are dynamic structures that control the exchange between ER and mitochondria of ions and lipids, tuning complex biological processes such as ER stress, autophagy, cell death and maintenance of glucose homeostasis [21–23]. A pivotal role of MAMs is the regulation of Ca^{2+} fluxes from ER to mitochondria through IP3Rs [24]; thus, HK2 displacement from MAMs could affect intracellular Ca^{2+} dynamics, raising the possibility that a Ca^{2+} dyshomeostasis can ensue and damage neoplastic cells.

Design of a peptide that displaces HK2 from MAMs without affecting hexokinase enzymatic activity

To investigate this possibility and to generate a tool with a potential anti-tumor activity *in vivo*, we have conceived a HK2-targeting cell penetrating peptide (CPP), dubbed HK2pep (Fig 1G). HK2pep is designed with a modular structure composed of: (i) a N-terminal HK2 tail, which acts as the active moiety by displacing HK2 from the outer mitochondrial membrane (in the negative control, SCRpep, this HK2-specific sequence is substituted by a scrambled one); (ii) a polycation stretch required for plasma membrane permeation; (iii) a polyanion sequence that shields polycation charges; and iv) a matrix

metalloprotease 2 and 9 (MMP2/9) target sequence that links the two charged stretches. As previously observed with similar actionable CPPs [25], the metalloprotease target sequence inhibits cell uptake of the peptide until its polycation sequence is unmasked by MMP2/9 cleavage. MMPs are highly expressed in a variety of tumor types, where they induce extracellular matrix remodeling and favor cancer cell invasiveness [26]. Hence, HK2pep should be preferentially activated inside neoplasms, and its subsequent entry through the plasma membrane would then lead to HK2 displacement from mitochondria and eventually cancer cell death. Moreover, HK2pep is not permeable across the endothelium of normal blood vessels, but its dimension (about 5 kDa) allows passage across the fenestrated endothelium that perfuses many cancer types.

The active moiety of HK2pep (i.e., the cleaved peptide, cl-HK2pep, Fig 1G) is indeed able to enter cells, to interact with mitochondria (Fig EV2A), and to induce HK2 detachment from MAMs in < 2 min (Figs 1H and EV2B). cl-HK2pep does not perturb hexokinase enzymatic activity either on the purified enzyme (Fig 1I) or on cell samples, where it is equally ineffective on HK2 and on the widespread isozyme HK1 (Figs 1J and EV2C). Moreover, the use of a subtoxic peptide concentration indicates that it does not affect the glycolytic activity of the target cell (Fig EV2D).

HK2 detachment from MAMs elicits a Ca^{2+} flux into mitochondria via IP3Rs and plasma membrane that causes mitochondrial depolarization

In accord with a role played by several MAM proteins in the regulation of Ca^{2+} homeostasis, cl-HK2pep prompts cycles of ER Ca^{2+} release and refill (Fig 2A) and boosts cytosolic IP$_3$ levels (Fig 2B). This IP$_3$ rise is prevented by pre-incubation with the IP3R inhibitor Xestospongin C (Xe-C; Fig 2B) and by chelating cytosolic Ca^{2+} (Fig EV3A), and delayed with respect to the Ca^{2+} release from ER (compare Fig 2A and B). These observations are consistent with cl-HK2pep eliciting a primary Ca^{2+} efflux from ER that prompts a surge in cytosolic IP$_3$ [27]. Indeed, Ca^{2+} enhances PLC activity that generates IP$_3$ [28], further amplifying ER Ca^{2+} release via IP3Rs.

Mitochondria can promptly take up Ca^{2+} released from ER, resulting in modulation of the activity of Krebs cycle enzymes and preventing deregulated increases in cytosolic [Ca^{2+}] [24,29]. cl-HK2pep treatment rapidly boosts mitochondrial [Ca^{2+}] in a stable and Xe-C-sensitive way (Movie EV1 and Fig 2C–E), rising mitochondrial [Ca^{2+}] to about 50 μM (Fig 2F). However, chelation of extracellular Ca^{2+} only induces a transient mitochondrial [Ca^{2+}] peak of about 12 μM (Fig 2F), indicating that cl-HK2pep administration elicits both Ca^{2+} release from ER and Ca^{2+} entry through plasma membrane, probably as a secondary effect [30], and that mitochondria take up Ca^{2+} from both sources. HK2 targeting also prompts a sudden and massive mitochondrial depolarization (Fig 2G and H, Movies EV2 and EV3 and Fig EV3B–E), which follows the increase in mitochondrial [Ca^{2+}] (Fig EV3F and G). This depolarization is inhibited by chelating cytosolic or extracellular Ca^{2+} and by the IP3R inhibitor Xe-C (Fig 2I and J, Movie EV4 and Fig EV3H).

Therefore, the HK2-targeted peptide causes mitochondrial Ca^{2+} overload as a consequence of Ca^{2+} release form ER via IP3Rs and of Ca^{2+} entry through plasma membrane. This signaling is further supported by the observation that HK2 co-immunoprecipitates with GRP75 (Fig EV3I), a chaperone that directly interacts with IP3R at
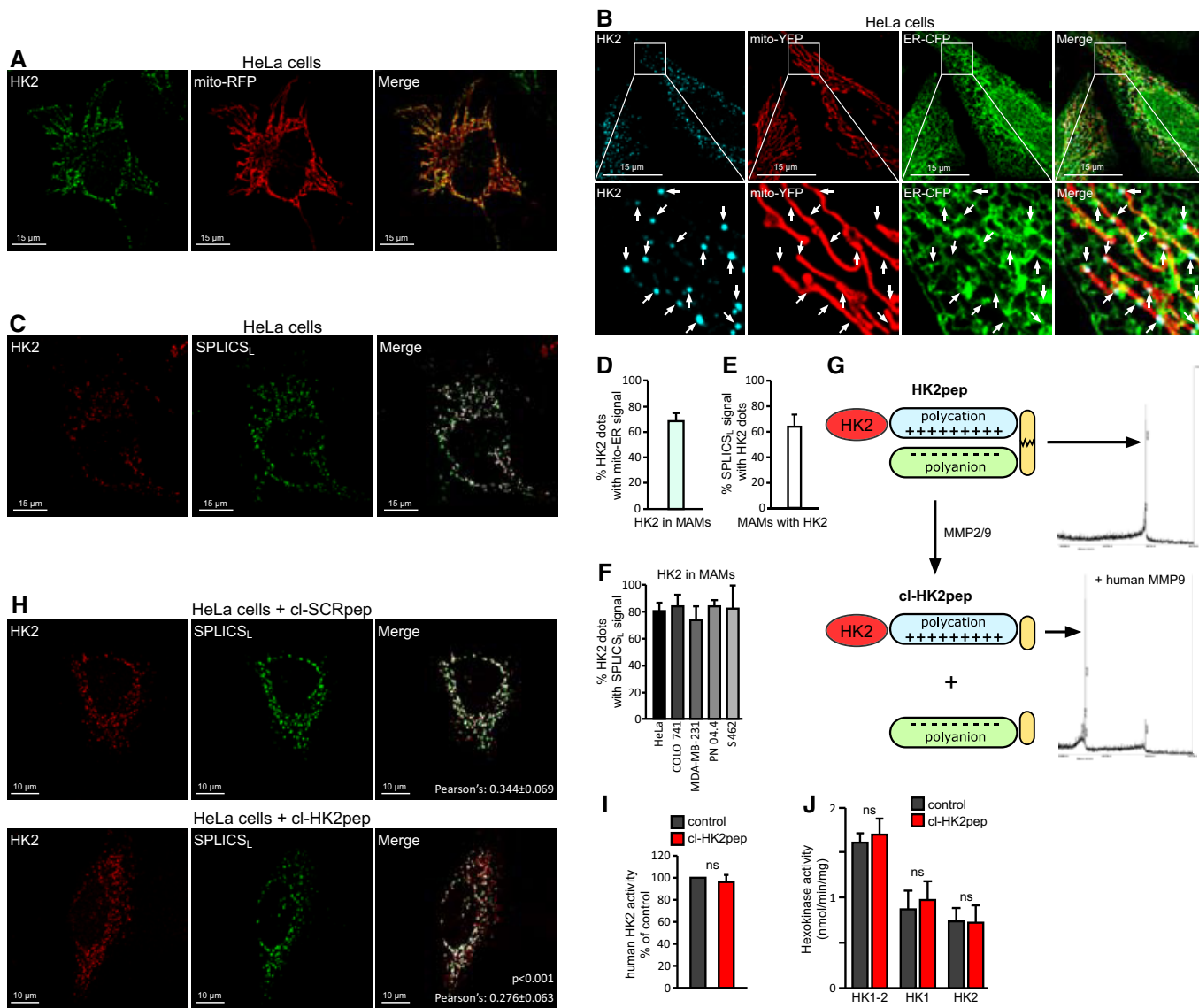
Figure 1. HK2 locates in MAM of cancer cells and is displaced by HK2pep.

A   Immunofluorescence staining of HK2 with an AlexaFluor488-conjugated antibody in HeLa cells expressing mitochondria-targeted RFP. Yellow signals in the merge analysis indicate mitochondrial localization of HK2. Scale bar: 15 μm.

B   Immunofluorescence staining of HK2 with a secondary AlexaFluor555-conjugated antibody in HeLa cells expressing both mitochondria-targeted YFP and ER-targeted CFP. The merged white signal indicates MAM localization of HK2 and is quantified in the bar graph on the right ($n = 24$). Image magnifications are shown in the lower part of the panel; arrows indicate HK2 dots in mito-ER contact sites. Scale bar: 15 μm.

C   Fluorescence co-staining of HK2 and split-GFP-based probe for ER-mitochondria contacts (SPLICS$_L$) on HeLa cells; HK2 is revealed with a secondary AlexaFluor555-conjugated antibody, and the merged signal is white. Scale bar: 15 μm.

D   Quantification of panel B experiment showing the percentage of HK2 dots that merge with MAMs in HeLa cells ($n = 24$ cells analyzed from three independent experiments; mean ± SD).

E   Quantification of panel C experiment showing the percentage of SPLICS$_L$ dots positive for HK2 in HeLa cells ($n = 10$ cells analyzed from three independent experiments; mean ± SD).

F   Percentage of HK2 dots positive for SPLICS$_L$ in HeLa, COLO 741, MDA-MB-231, PN 04.4, and S462 cells ($n \geq 6$ cells for each cell line; mean ± SD).

G   Functional unit composition of HK2pep (left); the HK2-targeting sequence is in red; the polycation and polyanion stretches are in light blue and light green, respectively; the MMP2/9 target sequence is in yellow. On the right, mass spectrometry profile of HK2pep before and after incubation (cl-HK2pep) with human MMP9.

H   HK2 displacement from HeLa MAMs after a 2 min treatment with cl-HK2pep is shown by loss of merging signal analyzed as in (C). cl-SCRpep is used as a negative control, and Pearson's co-localization coefficient is indicated in figure (cl-SCRpep $n = 26$ cells; cl-HK2pep $n = 24$ cells; $P < 0.001$ with a Student's t-test). Scale bar: 10 μm.

I, J   Effect of cl-HK2pep on glucose phosphorylation by human recombinant HK2 (I) or in 4T1 cell extracts (J), where both total hexokinase activity and HK1/HK2 specific activities are measured.
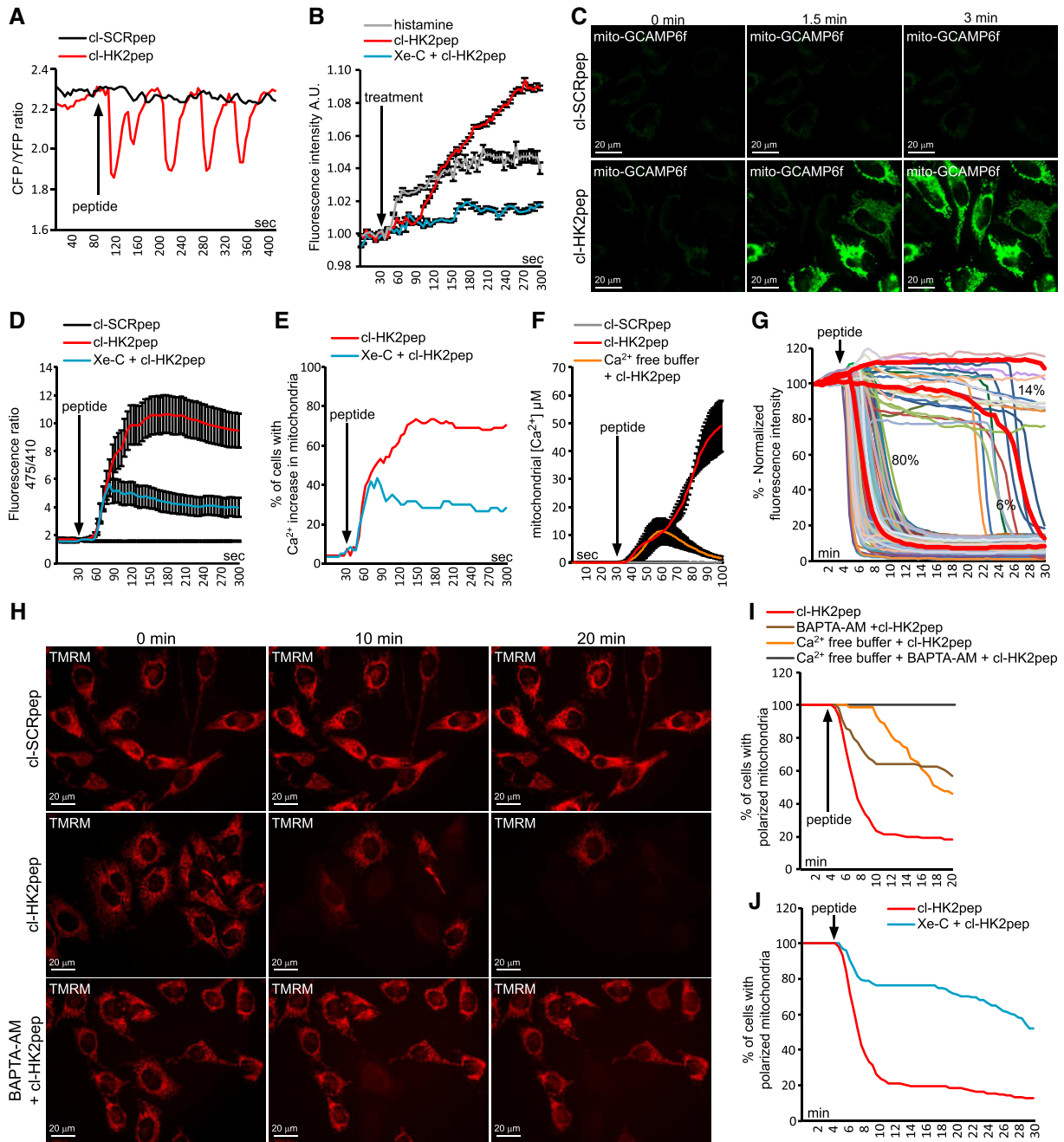
Figure 2. HK2 detachment from MAMs prompts Ca²⁺ influx and depolarization in mitochondria following IP3R opening.

A–F Effect of cl-HK2pep on cellular Ca²⁺ dynamics and IP₃ levels. ER Ca²⁺ levels are measured by the FRET-based, D4ER fluorescent probe expressed in the lumen of ER (A); IP₃ levels are assessed with the GFP-PHD probe; histamine (100 μM) is used as a positive control for IP₃ generation; data are reported as mean of fluorescent signals ± SEM (n = 3 independent experiments; B); changes in mitochondrial Ca²⁺ levels are recorded (C; scale bar: 20 μm) and quantified using the GCAMP6f sensor (in D, as mean of 475/410 nm ratio; signal ± SEM of at least five independent experiments and more than 20 cells analyzed), in (E) as percentage of cells with increased Ca²⁺ in mitochondria, with a threshold 475/410 ratio for positivity > 3; baseline mean ratio = 1.84 ± 0.54) or with mitochondria-targeted aequorin (F, where data are reported as mean of [Ca²⁺] ± SEM of 3 independent experimental days).

G–J Effect of cl-HK2pep treatment on mitochondrial membrane potential assessed with the TMRM probe. Kinetic experiments (G, single cell analysis, n = 216 cells analyzed in at least 10 independent experiments; H, representative field; scale bar: 20 μm) are quantified (I and J; TMRM fluorescence is normalized to initial value and expressed in percentage for each time point, with a depolarization threshold placed at 40% of initial value).

Data information: Experiments throughout the figure are carried out on HeLa cells; cl-SCRpep, negative control of cl-HK2pep (2 μM each). Where indicated, cells are kept in Ca²⁺-free medium plus 500 μM EGTA with or without 10 μM BAPTA-AM; Xe-C is Xestospongin C, which selectively inhibits IP3R at the 5 μM concentration used here [46].

MAMs and favors mitochondrial Ca^{2+} uptake upon IP_3-dependent Ca^{2+} release from the ER. This interaction is in line with the observation that HK2 locates to loose mitochondria-ER contacts sites (Fig 1C and F), which can accommodate the bulky IP3R-Grp75-VDAC complexes [24].

The HK2-targeting peptide triggers calpain-dependent cell death

Overcoming the efflux and the buffering capacity of Ca^{2+} in mitochondria can induce the permeability transition pore (PTP), a high conductance channel the opening of which commits cells to death [31,32]. PTP opening is independently inhibited by two unrelated molecules, Cyclosporin-A (CsA) and C63, but this inhibitory effect can be overwhelmed by intense stimuli of PTP induction [33]. We find that both CsA and C63 do not affect mitochondrial Ca^{2+} uptake following cl-HK2pep treatment (Fig 3A), but markedly delay mitochondrial depolarization (Fig 3B and Movies EV5 and EV6), indicating that this occurs downstream to PTP induction.

The HK2-targeting peptide abruptly elicits cell death in all tested cancer cell models (Fig 3C). The effect of cl-HK2pep did not change when cells were kept in the absence of glucose or were treated with HK inhibitors (Fig EV4A and B), indicating that it is independent of HK2 enzymatic activity. Peptide administration triggers mitochondrial depolarization in most tumor cells after 2–4 min, followed by phosphatidylserine exposure on the cell surface and plasma membrane rupture in < 1 h (Fig 3D and E, Movie EV7). Even though these are typical apoptotic changes, none of them is affected by the pan-caspase inhibitor Z-VAD-fmk (Figs 3E and EV4C–E). However, the broad-spectrum calpain inhibitor PD150606 abrogates cl-HK2pep-dependent induction of mitochondrial depolarization and cell death (Figs 3E–G and EV4F–L) without affecting the mitochondrial Ca^{2+} rise triggered by the peptide (Fig 3H). Taken together, these data indicate that HK2 displacement from MAMs does not trigger a classical apoptotic pathway, but rather activates a cell death process relying on the Ca^{2+}-dependent proteases calpains [34]. We also evaluated the effect of cl-HK2pep administration on non-transformed cell types. Mouse RAW 264.7 macrophages and mouse C2C12 myoblasts express HK2 (Fig EV4M), even though it is barely located in MAMs (Fig EV4N). Treatment with cl-HK2pep is poorly effective in inducing death of these cell models (Fig EV4O and P), and it does not elicit any apoptosis in HK2-negative hepatocytes (Fig EV4Q).

The HK2-targeting peptide kills primary B-chronic lymphatic leukemia (B-CLL) cells and inhibits neoplastic growth of colon and breast cancer cells

In order to test its efficacy as a potential anti-neoplastic treatment, we studied the effect of cl-HK2pep on freshly isolated leukemia cells obtained from B-CLL patients. B-CLL is the most common leukemia form that accounts for about 40% of all adult leukemias [35]. Although in the last years several new molecules, including anti-CD20 antibodies as well as kinase inhibitors, have become available for B-CLL therapy, the disease remains incurable and B-CLL patients usually relapse and/or become refractory. Induction of HK2 contributes to rituximab resistance [36], and release of MMP9 increases motility of B-CLL cells [37]; hence, B-CLL constitutes an interesting model for testing the effectiveness of HK2pep. HK2 is poorly detectable in non-transformed B cells, whereas it is expressed in B-CLL cells of all patients that we have analyzed (Fig 4A and B) independently of their mutation status (Table 1). All these patients' cells undergo a massive mitochondrial depolarization and cell death in the first 15 min of cl-HK2pep treatment (Fig 4C–E). These events are calpain-dependent (Fig 4C–E) and in all analyzed samples HK2 targeting completely erases B-CLL cells (Fig 4F), whereas it is less effective in inducing death in non-neoplastic, $CD19^+$ B cells (Fig 4G).

We have then evaluated the effect of targeting HK2 on solid tumors. Silencing HK2 expression hampers the ability of cancer cells to form colonies (Fig 5A and B), and HK2 targeting with both cl-HK2pep and the entire HK2pep inhibits *in vitro* tumorigenic growth by killing cancer cells (Fig 5C and D). Efficacy of the entire HK2pep indicates that its active moiety is released by MMP2/9 cleavage and that this peptide can be used on *in vivo* neoplastic models in which HK2 and MMP2/9 are expressed (Figs 5E and EV5A). We observe that intratumor injections of either cl-HK2pep or entire HK2pep significantly decrease the volume of allograft-injected colon cancer cells (Fig 5F), and the same result is achieved by intraperitoneal injection of entire HK2pep on both colon and breast cancer allografts (Figs 5G and H, and EV5C and D, Movies EV8 and EV9). Peptide administration does not cause any harm in treated animals, as assessed by lack of weight loss and of tissue damage (Fig EV5B and E), whereas it decreases mitotic index and enhances apoptosis inside tumor masses (Fig EV5F).

Our results indicate that HK2 specifically locates in MAMs and that unhinging HK2 from MAMs swiftly elicits calpain-dependent

---

Figure 3. HK2pep induces PTP- and calpain-dependent cell death.

A, B Effects of the PTP desensitizers CsA or C63 (5 μM each, 1 h pre-incubation) on mitochondrial Ca^{2+} levels recorded with GCAMP6f (A) and on mitochondrial membrane potential assessed with TMRM (B) in cells treated with cl-HK2pep.

C–F Cell death induction by cl-HK2pep; in the cytofluorimetric analyses reported in C, E, and F, viable cells are double negative for Annexin V-FITC and 7-AAD staining and measured 15 min after peptide treatment; in the kinetic experiment shown in D (scale bar: 50 μm), viable cells are double negative for Annexin V-FITC and 7-AAD and TMRM positive. In C and F, data are presented as mean ± SD and they were obtained from 3 different experiments or more; 3 technical replicates in all analyzed experiment.

G, H Effect of calpain inhibition on mitochondrial membrane potential assessed with TMRM (G, normalized fluorescence signal mean ± SD; three different experiments including three technical replicates each) and on mitochondrial Ca^{2+} levels recorded with GCAMP6f (H) in cells treated with cl-HK2pep.

Data information: Experiments throughout the figure are carried out on HeLa cells; cl-SCRpep, negative control of cl-HK2pep (2 μM each), where indicated, the caspase inhibitor Z-VAD-fmk or the calpain inhibitor PD150606 (50 μM each) are pre-incubated 1 h before peptide treatment. Experiments using TMRM or GCAMP6f probes are analyzed as in Fig 2. In C, F, and G, data are presented as mean ± SD of at least three independent experiments. In C ***P < 0.001 with Student's *t*-test; in F and G, P < 0.0001 with a two-way ANOVA (cl-HK2pep treatment versus cl-HK2pep+PD150606 or cl-SCRpep treatments); Bonferroni post-test in graph ***P < 0.001 (cl-HK2pep versus cl-SCRpep and cl-HK2pep versus PD150606 + cl-HK2pep).
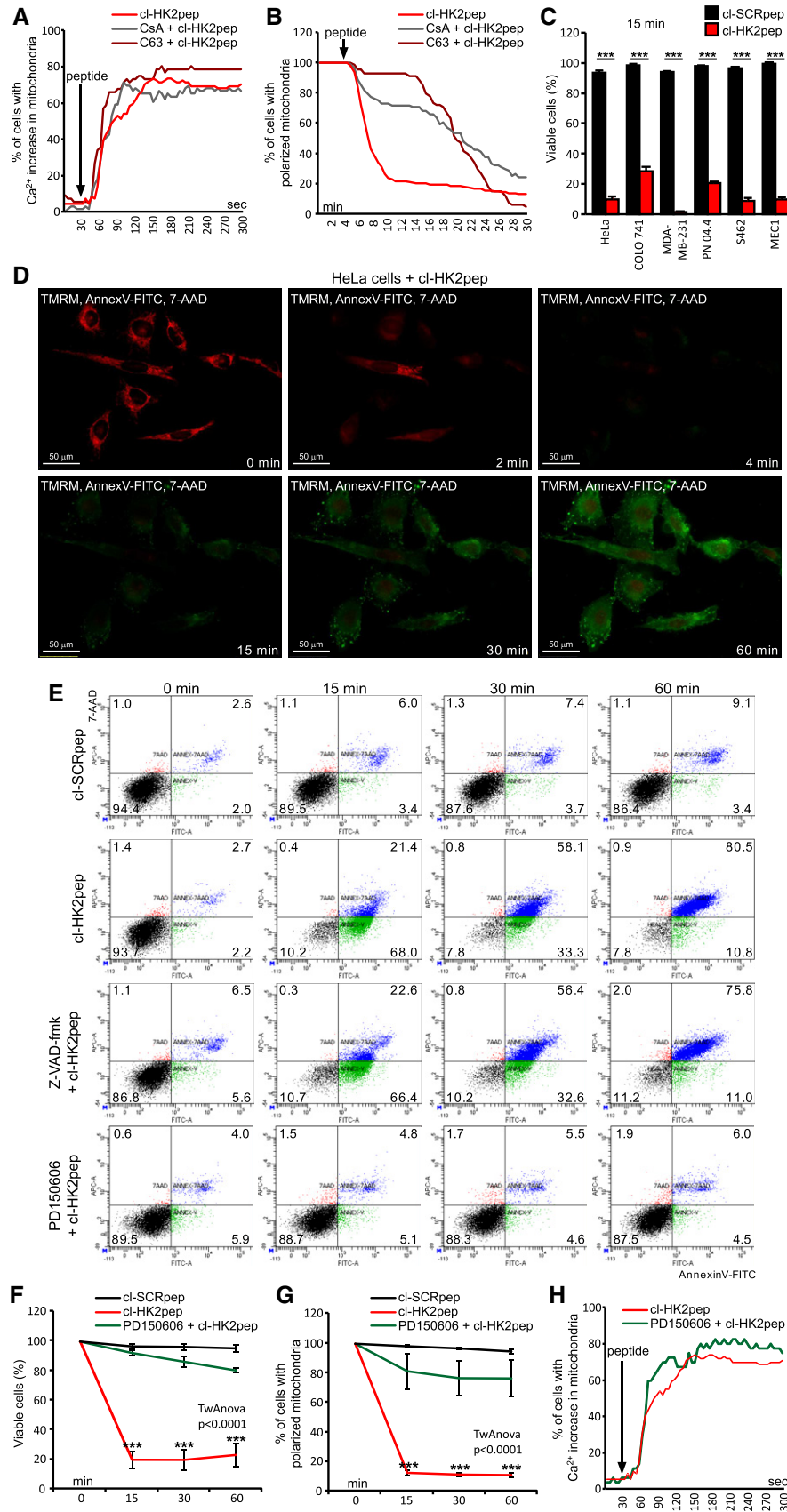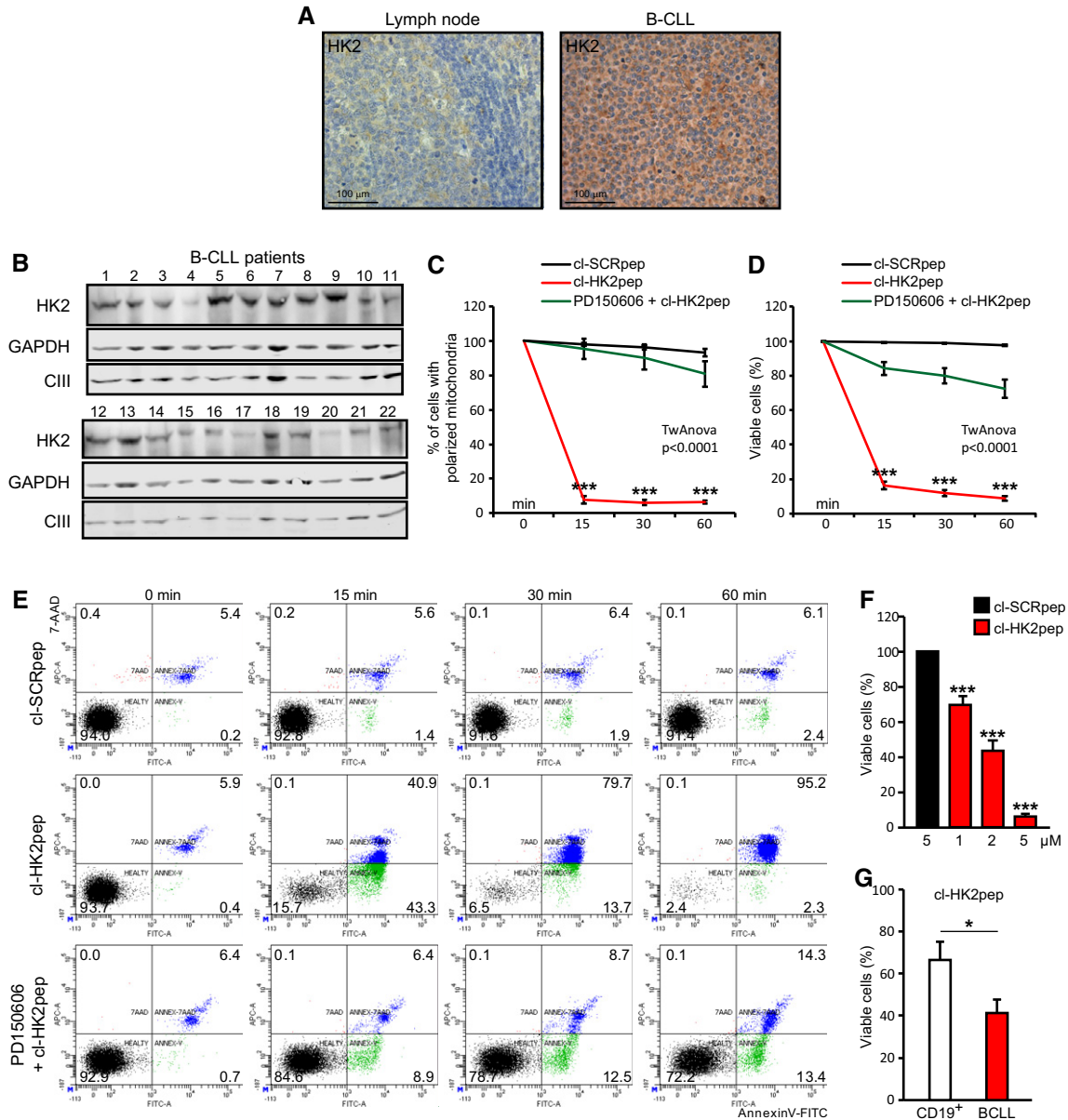
Figure 3.

Figure 4. HK2pep kills primary B-CLL cells.

A   Representative IHCs in human reactive lymphoid tissue, where HK2 expression is mainly restricted to proliferating blasts within germinal centers (center) and in patient B-CLL cells. Scale bar 100 μm.

B–G   Effect of cl-HK2pep on human B-CLL cells freshly isolated from patients. HK2-expressing B-CLL cells (B; GAPDH and respiratory complex III subunit UQCRC2 are cytosol and mitochondrial loading controls, respectively) undergo mitochondrial depolarization assessed by TMRM staining (C) and cell death, measured by cytofluorimetric analysis of Annexin V-FITC and 7-AAD staining (D-G). Cells are treated with 5 μM cl-HK2pep; PD150606 (50 μM) is pre-incubated for 1 h. Experiments are carried out on samples from at least 10 patients and on CD19^{+}, primary B lymphocytes from 5 healthy controls. In C, D, F, and G, data are presented as mean ± SEM; all data were obtained from three technical replicates in all analyzed patient samples. In (C, D) two-way ANOVA: $P < 0.0001$ (cl-HK2pep treatment versus cl-HK2pep+PD150606 or cl-SCRpep treatments); Bonferroni post-test in graph ***$P < 0.001$ (cl-HK2pep versus cl-SCRpep and cl-HK2pep versus PD150606+cl-HK2pep), in F and G, Student's t-test; ***$P < 0.01$, *$P < 0.05$.

death in cancer cells by funneling Ca^{2+} into mitochondria from ER and extracellular milieu. This signaling pathway is unprecedented, even though it is consistent with emerging evidences of a role played by MAMs in the maintenance of glucose homeostasis [23]. We unveil a role of HK2 in handling intracellular Ca^{2+} fluxes, which suggests that HK2 can act as a regulatory hub to integrate glucose metabolism with Ca^{2+}-mediated biochemical events, spanning from physiological responses to metabolic fluctuations to death induction under stress conditions. Hence, HK2 could contribute to the orchestration of the biochemical crosstalk between ER and mitochondria, with relevant

Table 1. Biological and clinical characteristics of the 22 B-CLL patients analyzed.

Median age, years (range)	74 (62–86)
Male/Female	12/10
WBC count,/mm^3 (range)	72,435 (21,410–168,940)
Lymphocytes, % (range)	80 (58-92)
Mutated[a]	14/22
Karyotype (N[b]/13q-/12 + /11q-/17p-)	3/15/3/0/1

WBC, white blood cell.
[a]Mutated was defined as having a frequency of mutations > 2% from the germline IGHV sequence.
[b]N = normal karyotype.

implications both in the physiology and in several pathological conditions of HK2-expressing tissues, including diabetes, ischemic damage of the heart or muscle wasting diseases, notwithstanding tumors.

HK2 shuttling to mitochondria is modulated by Akt-dependent threonine phosphorylation [11] and HectH9-dependent, non-proteolytic lysine ubiquitination [38]. These data place mitochondrial localization of HK2 in a multifaceted network of regulatory events, and the functional interaction between HK2 and IP3Rs that we observe further adds to this network. A thorough dissection of the dynamic modulation of these interactions will be instrumental for the comprehension of the effects of HK2 displacement from MAMs. Importantly, non-tumor cells expressing HK2 are much more refractory to peptide toxicity than neoplastic cells. This is a promising observation under a therapeutic perspective. Nonetheless, it is necessary to understand whether MAM composition differs between tumor and non-tumor cells, and how this affects HK2 activity and localization, as well as to connect cell response to HK2pep to the pattern of calpain expression, in order to draw an exhaustive picture of the mode of peptide action and to preview its effectiveness in specific settings.

The use of CPPs as vectors for the delivery of molecules with anti-cancer activity constitutes an active field of investigation, even though the transfer of this approach to the clinical practice has been hampered up to now by several shortcomings, such as
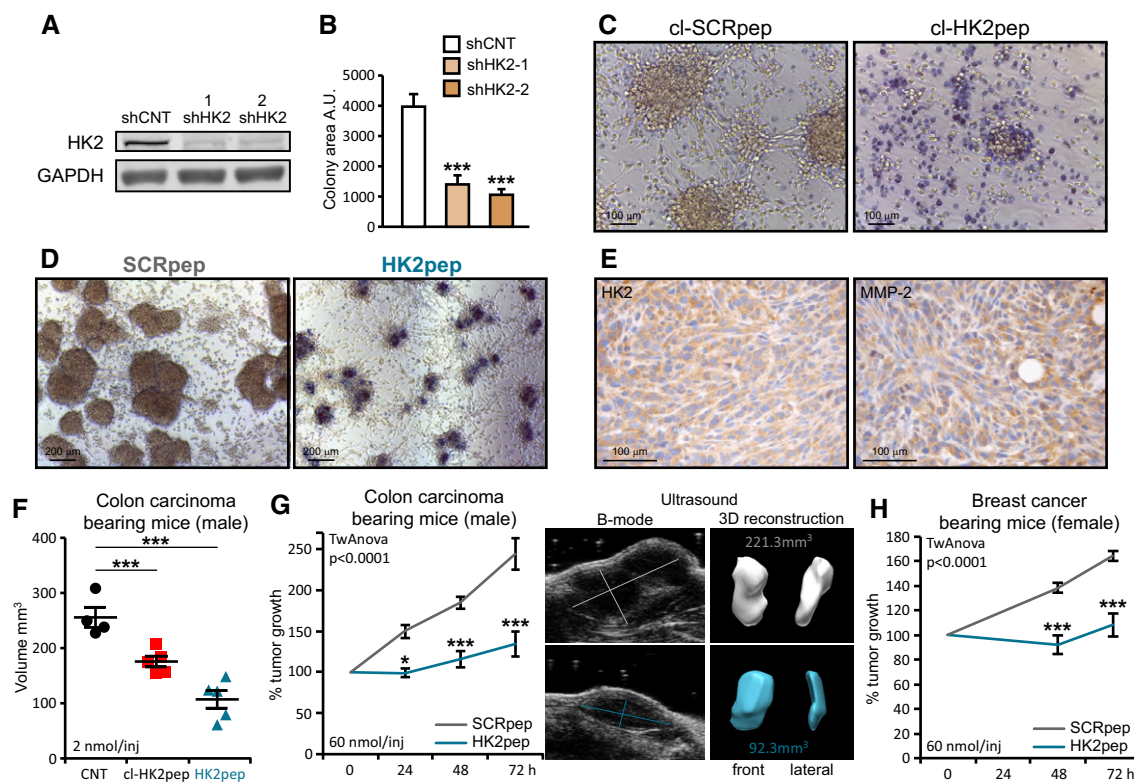
Figure 5. The HK2-targeting peptide inhibits *in vitro* and *in vivo* tumor growth.

A–D Effect of HK2 targeting on *in vitro* tumorigenicity. HK2 silencing with two different shRNAs (shHK2-1 and shHK2-2) in CT26 colon cancer cells (A) inhibits growth in soft agar (B; colony area ± SEM; n = 6 replicates obtained from three independent experiments; Student's *t*-test ***P < 0.001; A.U., arbitrary units). Treatment with cl-HK2pep (50 μM, 6 h; C, scale bar: 100 μm) or with the uncleaved HK2pep (2 μM, 48 h; D, scale bar: 200 μm) reverts formation of foci; dead cells are highlighted by Trypan Blue staining.

E–H Effect of HK2-targeting on *in vivo* neoplastic growth. HK2- and MMP-2-expressing CT26 cells (E, scale bar: 100 μm) are allografted in Balb/c male mice. Intratumor administration (5 injections of 2 nmol peptide every 12 h) of either cl-HK2pep or HK2pep (F; CNT n = 4; cl-HK2pep n = 5; HK2pep n = 5 mice), or intraperitoneal administration of HK2pep (G; 5 injections of 60 nmol peptide every 12 h; SCRpep n = 6; HK2pep n = 7 mice) reduce neoplastic growth; the same effect is observed on allografts of breast carcinoma 4T1 cells (H; 5 injections of 60 nmol peptide every 12 h; SCRpep n = 5; HK2pep n = 7 mice) in Balb/c female mice.

Data information: Throughout the figure, cl-SCRpep or SCRpep are used as peptide negative control. In G, representative ultrasound inspections and 3D reconstructions of tumor masses are shown (light gray: SCRpep treated animal; light blue: HK2pep treated animal). In F, mean tumor volume ± SD is reported; Student's *t*-test ***P < 0.001; in G, H, normalized volume ± SEM; a two-way ANOVA is performed (P < 0.001 - HK2pep versus SCRpep); Bonferroni post-test in the graphs *P < 0.05; ***P < 0.001.

the lack of cell specificity and the short duration of action [39]. Here, we combine several strategies to overcome these limitations. HK2pep is an activatable peptide composed by assembled modular units that can be adapted to the specific tumor(s) to be targeted. The MMP2/9 cleavage site allows the selective activation of HK2pep where these metalloproteases are highly expressed, as in the microenvironment of several tumors, but cleavage sites for other extracellular matrix components can be envisaged and tailored to specific neoplastic types. The limited size of HK2 pep (< 5 kDa) allows its passage through the fenestrated endothelium that characterizes many malignancies, and the rapidity of action of its cleaved form can circumvent problems connected with timing of degradation or excretion. Moreover, the absence of any inhibitory effect of HK2pep on the enzymatic activity of hexokinases minimizes the risk of non-specific damage caused by alterations of glucose metabolism at secondary sites. Hence, our approach to displace HK2 from MAMs integrates selectivity, efficacy, and lack of off-target effects and could be evolved toward the development of novel anti-neoplastic strategies, conceivably in combination with other chemotherapeutic approaches that target different liabilities of neoplastic cells.

Materials and Methods

Cell culture and HK2 silencing

Human cervix carcinoma HeLa cells, human breast cancer MDA-MB-231 cells, human malignant peripheral nerve sheath tumor S462 cells, human plexiform neurofibroma PN 04.4 cells, mouse breast cancer 4T1 cells and mouse colorectal carcinoma CT26 cells, mouse macrophage RAW 264.7 cells and, mouse myoblast C2C12 cells were cultured in DMEM medium (Gibco); colorectal carcinoma COLO 741 cells and B-CLL MEC1 cells were cultured in RPMI 1640 medium (Gibco); both culture media were supplemented with 10% fetal bovine serum (Gibco), glutamine 2 mM (Gibco), and penicillin–streptomycin (100 μg/ml; Invitrogen) and were kept at 37°C in a 5% CO_2 humidified atmosphere.

HKII expression was stably interfered by infecting cells with a lentivirus carrying the following shRNAs (Sigma) against mouse HKII mRNA:

(1) CCGGCATCACCCTGCTGGTTCTAAACTCGAGTTTAGAACCAG CAGGGTGATGTTTTTG;
(2) CCGGCGGTACAGAGAAAGGAGACTTCTCGAGAAGTCTCCTT TCTCTGTACCGTTTTTG.

Scrambled shRNA (Sigma) was used as negative control. Transduced cells were selected in 1.0 μg/ml puromycin.

Histological and immunohistochemical analyses

Histological and immunohistochemical analyses were performed both on primary human samples (colorectal carcinoma, $n = 6$; breast carcinoma, $n = 6$; MPNST, $n = 6$; lymph nodes deriving from B-cell chronic lymphocytic leukemia patients, $n = 6$) and on samples derived from mouse tumor models (PN tumors; CT26 and 4T1 subcutaneous grafts in Balb/c mice). In detail, 4-μm-thick tissue sections were obtained from formalin-fixed paraffin-embedded tissue samples

and representative tumor areas were selected on H&E-stained slides for immunohistochemical (IHC) analysis. IHC was performed using primary goat polyclonal anti-HK2 (sc-6521, Santa Cruz) and rabbit monoclonal anti-MPP2 (ab92536, Abcam) antibodies. Antigen retrieval was performed with heat/EDTA in the Bond-Max automated immunostainer (Leica Biosystems), as previously described [40].

Cell lysates and Western immunoblot analysis

Cells lysis (5×10^5 for each assay) was performed in Tris 20 mM, NaCl 150 mM, EDTA 2 mM, EGTA 2 mM, and Triton X-100 0.5% supplemented with phosphatase and protease inhibitors (Sigma). Protein quantification was performed with BCA Protein Assay Kit (Thermo Scientific-Pierce). After SDS/PAGE gel electrophoresis, proteins were transferred onto nitrocellulose Hybond-C Extra membranes (Amersham, Uppsala; Sweden) and immunostained with goat polyclonal anti-HK2 (clone sc-6521, Santa Cruz), anti-GAPDH (#2118, Cell Signaling), ATP5A (ab14748, Abcam), anti-UQCRC2 (ab14745, Abcam), rabbit monoclonal anti-MMP2 (ab92536, Abcam), rabbit monoclonal anti-MMP9 (ab137867, Abcam) rabbit polyclonal, and TOM20 (sc-11415, Santa Cruz) antibodies.

Peptide synthesis

HK2pep, SCRpep, cl-HK2pep, and cl-SCRpep were synthesized by automatic solid-phase procedures using a multiple peptide synthesizer (SyroII, MultiSynTech GmbH) on a pre-loaded Wang resin (100–200 mesh) (Novabiochem). The fluoren-9-ylmethoxycarbonyl (Fmoc) strategy was used throughout the peptide chain assembly, utilizing O-(7-azabenzotriazol-1-yl)-N,N,N′,N′-tetramethyluronium hexafluorophosphate (HATU) as coupling reagent. The side-chain protected amino acid building blocks used were as follows: Fmoc-Tyr(tert-butyl), Fmoc-Glu(tert-butyl), Fmoc-Ser(tertbutyl), Fmoc-Thr(tert-butyl), Fmoc-His(trityl), Fmoc-Asn(trityl), and Fmoc- Arg (2,2,4,6,7-pentamethyldihydrobenzofuran-5-sulfonyl). Cleavage of the peptides was performed by reacting the peptidyl-resins with a mixture containing TFA/H20/thioanisole/ethanedithiol/phenol (10 ml/0.5 ml/0.5 ml/0.25 ml/750 mg) for 2.5 h. Crude peptides were purified by a preparative reverse-phase HPLC. Molecular masses of the peptide were confirmed by mass spectroscopy on a MALDI TOF-TOF using a Applied Biosystems 4800 mass spectrometer. The purity of the peptides was about 95% as evaluated by analytical reverse-phase HPLC. Peptide sequences:
HK2pep: MIASHLLAYFFTELN-βA-RRRRRRRRR-PLGLAG-Ahx-EEEE EEEE
SCRpep: VGAHAGEYGAEALER-βA-RRRRRRRRR-PLGLAG-Ahx-EEEE EEEE
cl-HK2pep: MIASHLLAYFFTELN-βA-RRRRRRRRR-PLG
cl-SCRpep: VGAHAGEYGAEALER-βA-RRRRRRRRR-PLG

Fluorescent peptide synthesis

Fluo-cl-HK2pep and fluo-cl-SCRpep were synthesized by microwave-assisted solid-phase procedures using a Biotage Alstra peptide synthesizer on a pre-loaded HMPB-resin (100–200 mesh-Iris Biotech GmbH). The fluoren-9-ylmethoxycarbonyl (Fmoc) strategy was used throughout the peptide chain assembly. Activation of entering Fmoc-

protected amino acids (0.3 M solution in DMF) was performed using 0.5 M Oxyma in DMF/0.5 M DIC in DMF (1:1:1 molar ratio), with a 5 equivalent excess over the initial resin loading. Coupling steps were performed for 7 min at 75°C. Fmoc-deprotection steps were performed by treatment with a 20% piperidine solution in DMF at room temperature (1 × 10 min). Following each coupling or deprotection step, peptidyl-resin was washed with DMF (4 × 3.5 ml). Upon complete chain assembly, resin was washed with DCM (5× 3.5 ml) and gently dried under a nitrogen flow. Resin-bound peptide was treated with an ice-cold TFA, TIS, water, and thioanisole mixture (90:5:2.5:2.5 v/v/v/v, 4 ml) for 2 h. Crude peptides were purified by a preparative reverse-phase HPLC. Molecular masses of the peptide were confirmed by mass spectroscopy using a Bruker Esquire 3000 + instrument equipped with an electro-spray ionization source and a quadrupole ion trap detector (QITD). The purity of the peptides was about 95% as evaluated by analytical reverse-phase HPLC. Peptide conjugation with fluorescent dyes (ATTO) was performed by reacting peptide thiol groups with maleimide-ATTO dyes. Briefly, peptides were dissolved at a 5 mg/ml concentration in PBS buffer (pH 7.2) and 1.1 equivalents of maleimide-dye were added to the solution. Reaction was monitored by HPLC until completion and then the product isolated by preparative HPLC.

HK2pep cleavage assay

Human recombinant MMP9 (911MP, R&D) was reconstituted following manufacturer's instructions in a buffer composed by 50 mM Tris, 150 mM NaCl, 10 mM $CaCl_2$, and 0.05% Brij−35 (w/v) at pH 7.5 and activated with p−aminophenylmercuric acetate (Sigma). hMMP9 (20 nM) was incubated for 4 h with 1 µg HK2pep in a final 100 µl volume; samples were analyzed by mass/spec as described above.

Measurement of hexokinase enzymatic activity

Hexokinase enzymatic activity was measured monitoring NADPH formation at 37°C with Infinite M200 spectrophotometer (TECAN) in a buffer containing 50 mM Tris, 10 mM $MgCl_2$, 4 mM ATP, 2 mM glucose, 0.1 U/ml G6PDH, and 1 mM NADP, pH 7.4. Experiments were carried out either using Human HK2 recombinant protein (0.5 µg; HXK0703, ATGEN) or total cell lysate (20 µg) were exposed for 30 min to 10 µM cl-HK2pep. To discriminate between HK1 and HK2 activities in cells, samples were heated to 46°C for 30 min in order to inactivate thermo-sensitive HK2 activity.

Immunofluorescence (IF) analyses

IF experiments were carried out 24 h after transfection with TransIT®-LT1 (Mirus) on cells fixed in 4% PFA, quenched with NH_4Cl (0.24% in PBS), and permeabilized with 0.1% Triton X-100.

Primary antibodies (rabbit monoclonal anti-HK2, H.738.7, Thermo Scientific; mouse monoclonal anti-TOM20, sc-17764, Santa Cruz) were diluted 1:150 in blocking solution (2% BSA, 10% goat serum, and 0.2% gelatin in PBS) and incubated for 90 min, at RT; AlexaFluor488/555/647-conjugated secondary antibodies (Life Technologies) were diluted 1:300 in blocking solution and incubated 45 min at RT. Images were collected on a Leica SP5-II confocal microscope and equipped with a 100×/1.4 N.A. Plan Apochromat objective. A WLL laser was used to excite each specific dye, and a

HyD (Leica) was employed for signal collection. After background subtraction, Pearson's co-localization coefficient was calculated with the *ImageJ Co-localization* Analysis plugin. Displayed images were processed with the automatic ImageJ plugin *Enhance image* to improve signal intensity, but analyses were performed on raw, background-subtracted data. For measurements of co-localization with the split-GFP-based probe for ER-mitochondria contacts (SPLICS$_L$) [20], TOM20 and HK2 channels were background subtracted, a threshold (the mean fluorescence intensity for each cell) was imposed, and the % of pixels co-localized with SPLICS$_L$ was calculated, as described [41]. The plasmids encoding mt-YFP, mt-RFP, and ER-CFP were previously described [41].

Mitochondrial Ca^{2+} measurements

For FRET-based ER Ca^{2+} measurements, cells were transfected with the ER-targeted D4ER Ca^{2+} probe and mounted into an open-topped chamber in Krebs–Ringer modified buffer (mKRB, in mM: 140 NaCl, 2.8 KCl, 2 $MgCl_2$, 10 HEPES, 11 glucose, pH 7.4 at 37°C) supplemented with $CaCl_2$ 1 mM; imaging was performed with a DM6000 inverted microscope (Leica, HCX Plan Apo 40 × oil objective, NA 1.25), as previously described [42]. Excitation light was generated every 5s by a 410 nm LED (Led Engin LZ1-00UA00 LED). ImageJ was used for off-line analysis of FRET experiments. YFP and CFP images were background-subtracted and analyzed selecting specific regions of interest (ROIs) on each cell. The ratio (R) between YFP and CFP emissions was calculated for each frame.

For GCAMP6f Ca^{2+} measurements, cells were transfected with a cDNA encoding mitochondrial and nuclear GCAMP6f [41]. To perform Ca^{2+} measurements, medium was replaced with mKRB buffer supplemented with 1 µM CsH (Adipogen) and with 1 mM $CaCl_2$ or 500 µM EGTA. Where indicated, specific drugs were added to the buffer and pre-incubated for 30 min with BAPTA-AM (5 µM, Thermo Fisher Scientific) or 1 h with Xestospongin C (5 µM, Santa Cruz), CsA (5 µM, Sigma), C63 (5 µM), or PD150606 (50 µM, Calbiochem). Fluorescence was recorded with an inverted microscope (Zeiss Axiovert 100, Fluar 40× oil objective, NA 1.30) in the 500–530 nm range (by a band-pass filter, Chroma Technologies). Probes were sequentially excited at 475 nm and at 410 nm, respectively, for 180 and 300 ms, every 5 s. Excitation light, produced by a monochromator (polychrome V; TILL Photonics), was filtered with a 505 nm DRLP filter (Chroma Technologies). After background subtraction, images were analyzed with ImageJ, calculating the ratio (R) between emissions generated by exciting cells at 475 and 410 nm, respectively, in specific ROIs comprising the entire mitochondrial network. [Ca^{2+}] is proportional to R.

For aequorin Ca^{2+} measurements, cells were transfected with a plasmid encoding low-affinity mitochondrial matrix aequorin (mit-Aeqmut), which was reconstituted by incubating cells for 1 h in mKRB, supplemented with $CaCl_2$ 1 mM and native coelenterazine (5 µM, Biotium). Measurements were performed as previously described [41].

IP$_3$ measurement assay

In order to assess changes in intracellular IP$_3$ levels, cells were transfected with a plasmid encoding the GFP-tagged pleckstrin homology (PH) domain of PLC-δ1 (GFP-PHD). Quantification of IP$_3$

generation was evaluated as variations in cytosolic GFP-PHD fluorescence (F) normalized to initial cytosolic fluorescence (F0), due to the release of GFP-PHD from the plasma membrane upon PIP2 cleavage and IP_3 generation [43]. Only cells (~80%) in which a plasma membrane localization of GFP-PHD was evident were selected for analysis. Images were collected on a DM6000 inverted microscope (Leica, HCX Plan Apo 40× oil objective, NA 1.25). Excitation light was generated every 5 s by a 460 nm LED (Led Engin).

Measurements of mitochondrial membrane potential

Mitochondrial membrane potential was analyzed using the fluorescent potentiometric compound tetramethylrhodamine methyl ester (TMRM, 20 nM; Invitrogen). Cells were incubated in mKRB or DMEM without phenol red and with CsH (1 μM) to inhibit P-glycoproteins. Recordings were performed either with a fluorescence microscope (Olympus IX71 or Leica DMI600B) or with a flow cytometer (FACSCanto II, Becton Dickinson). For live microscope experiments, recordings were carried out every 30 sec using CellR software (Olympus) or LAS AF software (Leica). For flow cytometry analyses, TMRM signals are measured every 15 min and analyzed with FACSDiva software (Becton Dickinson). Movies were realized using CellR software (Olympus).

Cell viability assays

Cell viability was assessed either by cytofluorimetry or by fluorescence microscopy. Cytofluorimetric recordings of phosphatidylserine exposure on the cell surface (increased staining of FITC-conjugated Annexin V; Roche) and loss of plasma membrane integrity (7-AAD staining; Sigma) were repeated every 15 min on a FACSCanto II instrument and analyzed with FACSDiva software. Double-negative cells were considered viable. Fluorescence microscope recordings were performed with Leica DMI600B microscope and acquired with LAS AF software in the presence of Annexin V-FITC, 7-AAD, and TMRM pre-incubated for 45 min. Images and movie obtained with LAS AF software were analyzed with ImageJ software.

Isolation of B lymphocytes

Cell samples that matched standard morphological and immunophenotypic criteria for B-CLL were collected from 22 therapy-free patients after obtaining informed consent according to the Declaration of Helsinki. This study was authorized by the Ethics Committee of the Padova University Hospital (Approve Code: n. 3529/AO/14). Patient characteristics are reported in Table 1. Cells were separated by Ficoll-Hypaque gradient centrifugation (Euroclone), and B cells were purified from the PBMCs by removing T cells with the sheep erythrocyte rosetting method [44]. Untreated peripheral blood B cells were isolated from the PBMCs of healthy donors by negative selection with the RosetteSep for isolation of B cells (StemCell Technologies). All samples were used when they contained ≥ 95% $CD19^+$ cells, as assessed by flow cytometry.

In vitro tumorigenesis assays

For soft agar assays, cells in DMEM medium supplemented with 0.5% serum were mixed with low melting point agarose (Promega) at a final 0.6% concentration and plated on a bottom layer of DMEM with 1% LMP agarose. Fresh medium (DMEM 4% serum) was added every 3rd day. At day 15th, colonies were stained with Crystal Violet 0.005% and analyzed with ImageJ software.

For focus forming assays, cells were seeded in standard DMEM medium with 10% FBS, which was replaced with DMEM 0.5% FBS after cells reached confluence. Treatment with peptides was performed after formation of foci; dead cells were highlighted by Trypan Blue staining. Images were acquired using a Leica DMIL LED microscope equipped with a Leica ICC50 HD camera.

In vivo tumorigenesis assays

Colon cancer CT26 cells or breast cancer 4T1 cells were allografted in Balb/c mice according to a protocol approved from Italian Health Ministry (authorization number: 547/2016-PR). Briefly, 100,000 CT26 cells or 200,000 4T1 cells were injected subcutaneously in the flank of male or female animals, respectively, in a 100 μl final volume containing 30% Matrigel (Corning). Tumors were visible under the skin after 7–9 days and measured with caliper (two major axes). Tumor volume was calculated using the formula: $(a*b^2)/2$. Ultrasound inspections of representative tumors were performed using Vevo 2100 (Visualsonic, Fujifilm). Acquisitions, measurements, and 3D reconstructions of tumors were done using VevoLAB 1.7.0.7071 software. Peptides were injected as described in the text.

Measurements of extracellular acidification rate (ECAR)

In vivo ECAR was measured in order to assess changes in glycolytic activity in a kinetic mode on cell monolayers with an extracellular flux analyzer (Agilent Seahorse XF24), as described [45]. ECAR values were then normalized for the protein content of each sample.

Author contributions

Conceptualization, FCi, AR, and PB; Investigation, FCi, RF, IM, and MP; Resources, OM, ND, AG, FF, FCh, and LT; Formal Analysis, FCi and RF; Visualization, FCi and RF; Funding Acquisition, AR and PB; Supervision, FCi and AR; Project Administration, AR; Writing-Original Draft, AR; Writing-Review and Editing, AR, FCi, RF, PP, LT, PP, and PB.

Conflict of interest

A patent application was filed by University of Padova for the use of the HK2-targeting peptide described in the manuscript as an anti-neoplastic tool in in vitro and in vivo experiments.

References

1. Wilson JE (2003) Isozymes of mammalian hexokinase: structure, subcellular localization and metabolic function. *J Exp Biol* 206: 2049−2057

2. Vander Heiden MG, DeBerardinis RJ (2017) Understanding the intersections between metabolism and cancer biology. *Cell* 168: 657−669

3. DeWaal D, Nogueira V, Terry AR, Patra KC, Jeon SM, Guzman G, Au J, Long CP, Antoniewicz MR, Hay N (2018) Hexokinase-2 depletion inhibits glycolysis and induces oxidative phosphorylation in hepatocellular carcinoma and sensitizes to metformin. *Nat Comm* 9: 446

4. Robey RB, Hay N (2006) Mitochondrial hexokinases, novel mediators of the antiapoptotic effects of growth factors and Akt. *Oncogene* 25: 4683−4696

5. Wang L, Xiong H, Wu F, Zhang Y, Wang J, Zhao L, Guo X, Chang LJ, Zhang Y, You MJ *et al* (2014) Hexokinase 2-mediated Warburg effect is required for PTEN- and p53-deficiency-driven prostate cancer growth. *Cell Rep* 8: 1461−1474

6. Patra KC, Wang Q, Bhaskar PT, Miller L, Wang Z, Wheaton W, Chandel N, Laakso M, Muller WJ, Allen EL *et al* (2013) Hexokinase 2 is required for tumor initiation and maintenance and its systemic deletion is therapeutic in mouse models of cancer. *Cancer Cell* 24: 213−228

7. Bhalla K, Jaber S, Nahid MN, Underwood K, Beheshti A, Landon A, Bhandary B, Bastian P, Evens AM, Haley J *et al* (2018) Role of hypoxia in diffuse large B-cell lymphoma: metabolic repression and selective translation of HK2 facilitates development of DLBCL. *Sci Rep* 8: 744

8. Semenza GL (2013) HIF-1 mediates metabolic responses to intratumoral hypoxia and oncogenic mutations. *J Clin Invest* 123: 3664−3671

9. Mathupala SP, Ko YH, Pedersen PL (2009) Hexokinase-2 bound to mitochondria: cancer's stygian link to the "Warburg Effect" and a pivotal target for effective therapy. *Semin Cancer Biol* 19: 17−24

10. Roberts DJ, Tan-Sah VP, Ding EY, Smith JM, Miyamoto S (2014) Hexokinase-II positively regulates glucose starvation-induced autophagy through TORC1 inhibition. *Mol Cell* 53: 521−533

11. Miyamoto S, Murphy AN, Brown JH (2008) Akt mediates mitochondrial protection in cardiomyocytes through phosphorylation of mitochondrial hexokinase-II. *Cell Death Differ* 15: 521−529

12. Pantic B, Trevisan E, Citta A, Rigobello MP, Marin O, Bernardi P, Salvatori S, Rasola A (2013) Myotonic dystrophy protein kinase (DMPK) prevents ROS-induced cell death by assembling a hexokinase II-Src complex on the mitochondrial surface. *Cell Death Dis* 4: e858

13. Roberts DJ, Miyamoto S (2015) Hexokinase II integrates energy metabolism and cellular protection: akting on mitochondria and TORCing to autophagy. *Cell Death Differ* 22: 248−257

14. Mathupala SP, Ko YH, Pedersen PL (2010) The pivotal roles of mitochondria in cancer: Warburg and beyond and encouraging prospects for effective therapies. *Biochim Biophys Acta* 1797: 1225−1230

15. Wolf A, Agnihotri S, Micallef J, Mukherjee J, Sabha N, Cairns R, Hawkins C, Guha A (2011) Hexokinase 2 is a key mediator of aerobic glycolysis and promotes tumor growth in human glioblastoma multiforme. *J Exp Med* 208: 313−326

16. Suh DH, Kim MA, Kim H, Kim MK, Kim HS, Chung HH, Kim YB, Song YS (2014) Association of overexpression of hexokinase II with chemoresistance in epithelial ovarian cancer. *Clin Exp Med* 14: 345−353

17. Akins NS, Nielson TC, Le HV (2018) Inhibition of glycolysis and glutaminolysis: an emerging drug discovery approach to combat cancer. *Curr Top Med Chem* 18: 494−504

18. Chiara F, Castellaro D, Marin O, Petronilli V, Brusilow WS, Juhaszova M, Sollott SJ, Forte M, Bernardi P, Rasola A (2008) Hexokinase II

19. Masgras I, Rasola A, Bernardi P (2012) Induction of the permeability transition pore in cells depleted of mitochondrial DNA. *Biochim Biophys Acta* 1817: 1860−1866

20. Cieri D, Vicario M, Giacomello M, Vallese F, Filadi R, Wagner T, Pozzan T, Pizzo P, Scorrano L, Brini M *et al* (2018) SPLICS: a split green fluorescent protein-based contact site sensor for narrow and wide heterotypic organelle juxtaposition. *Cell Death Differ* 25: 1131−1145

21. Csordas G, Weaver D, Hajnoczky G (2018) Endoplasmic reticulum-mitochondrial contactology: structure and signaling functions. *Trends Cell Biol* 28: 523−540

22. Prudent J, McBride HM (2017) The mitochondria-endoplasmic reticulum contact sites: a signalling platform for cell death. *Curr Opin Cell Biol* 47: 52−63

23. Rieusset J (2018) The role of endoplasmic reticulum-mitochondria contact sites in the control of glucose homeostasis: an update. *Cell Death Dis* 9: 388

24. Filadi R, Theurey P, Pizzo P (2017) The endoplasmic reticulum-mitochondria coupling in health and disease: molecules, functions and significance. *Cell Calcium* 62: 1−15

25. Olson ES, Aguilera TA, Jiang T, Ellies LG, Nguyen QT, Wong EH, Gross LA, Tsien RY (2009) *In vivo* characterization of activatable cell penetrating peptides for targeting protease activity in cancer. *Integr Biol* 1: 382−393

26. Isaacson KJ, Martin Jensen M, Subrahmanyam NB, Ghandehari H (2017) Matrix-metalloproteinases as targets for controlled delivery in cancer: an analysis of upregulation and expression. *J Control Release* 259: 62−75

27. Rebecchi MJ, Pentyala SN (2000) Structure, function, and control of phosphoinositide-specific phospholipase C. *Physiol Rev* 80: 1291−1335

28. Horowitz LF, Hirdes W, Suh BC, Hilgemann DW, Mackie K, Hille B (2005) Phospholipase C in living cells: activation, inhibition, Ca^{2+} requirement, and regulation of M current. *J Gen Physiol* 126: 243−262

29. Cannino G, Ciscato F, Masgras I, Sanchez-Martin C, Rasola A (2018) Metabolic plasticity of tumor cell mitochondria. *Front Oncol* 8: 333

30. Berridge MJ, Bootman MD, Roderick HL (2003) Calcium signalling: dynamics, homeostasis and remodelling. *Nat Rev Mol Cell Biol* 4: 517−529

31. Rasola A, Bernardi P (2011) Mitochondrial permeability transition in Ca (2 +)-dependent apoptosis and necrosis. *Cell Calcium* 50: 222−233

32. Rasola A, Bernardi P (2014) The mitochondrial permeability transition pore and its adaptive responses in tumor cells. *Cell Calcium* 56: 437−445

33. Bernardi P, Rasola A, Forte M, Lippe G (2015) The mitochondrial permeability transition pore: channel formation by F-ATP synthase, integration in signal transduction, and role in pathophysiology. *Physiol Rev* 95: 1111−1155

34. Storr SJ, Carragher NO, Frame MC, Parr T, Martin SG (2011) The calpain system and cancer. *Nat Rev Cancer* 11: 364−374

35. Fabbri G, Dalla-Favera R (2016) The molecular pathogenesis of chronic lymphocytic leukaemia. *Nat Rev Cancer* 16: 145−162

36. Gu JJ, Singh A, Xue K, Mavis C, Barth M, Yanamadala V, Lenz P, Grau M, Lenz G, Czuczman MS *et al* (2018) Up-regulation of hexokinase II contributes to rituximab-chemotherapy resistance and is a clinically relevant target for therapeutic development. *Oncotarget* 9: 4020−4033

37. Martini V, Gattazzo C, Frezzato F, Trimarco V, Pizzi M, Chiodin G, Severin F, Scomazzon E, Guzzardo V, Saraggi D *et al* (2017) Cortactin, a Lyn substrate, is a checkpoint molecule at the intersection of BCR and

The top of the second column continues from reference 18:

detachment from mitochondria triggers apoptosis through the permeability transition pore independent of voltage-dependent anion channels. *PLoS ONE* 3: e1852

CXCR4 signalling pathway in chronic lymphocytic leukaemia cells. *Br J Haematol* 178: 81−93

38. Lee HJ, Li CF, Ruan D, He J, Montal ED, Lorenz S, Girnun GD, Chan CH (2019) Non-proteolytic ubiquitination of Hexokinase 2 by HectH9 controls tumor metabolism and cancer stem cell expansion. *Nat Commun* 10: 2625

39. Raucher D, Ryu JS (2015) Cell-penetrating peptides: strategies for anti-cancer treatment. *Trends Mol Med* 21: 560−570

40. Pizzi M, Agostinelli C, Righi S, Gazzola A, Mannu C, Galuppini F, Fassan M, Visentin A, Piazza F, Semenzato GC *et al* (2017) Aberrant expression of CD10 and BCL6 in mantle cell lymphoma. *Histopathology* 71: 769−777

41. Filadi R, Leal NS, Schreiner B, Rossi A, Dentoni G, Pinho CM, Wiehager B, Cieri D, Cali Pizzo P *et al* (2018) TOM70 sustains cell bioenergetics by promoting IP3R3-mediated ER to mitochondria Ca(2+) transfer. *Curr Biol* 28: 369−382 e366

42. Fedeli C, Filadi R, Rossi A, Mammucari C, Pizzo P (2019) PSEN2 (prese-nilin 2) mutants linked to familial Alzheimer disease impair autophagy by altering Ca(2+) homeostasis. *Autophagy* 15: 2044−2206

43. Hirose K, Kadowaki S, Tanabe M, Takeshima H, Iino M (1999) Spatiotem-poral dynamics of inositol 1,4,5-trisphosphate that underlies complex Ca2 + mobilization patterns. *Science* 284: 1527−1530

44. Frezzato F, Trimarco V, Martini V, Gattazzo C, Ave E, Visentin A, Cabrelle A, Olivieri V, Zambello R, Facco M *et al* (2014) Leukaemic cells from chronic lymphocytic leukaemia patients undergo apoptosis following microtubule depolymerization and Lyn inhibition by nocodazole. *Br J Haematol* 165: 659−672

45. Masgras I, Ciscato F, Brunati AM, Tibaldi E, Indraccolo S, Curtarello M, Chiara F, Cannino G, Papaleo E, Lambrughi M *et al* (2017) Absence of neurofibromin induces an oncogenic metabolic switch via mitochondrial ERK-mediated phosphorylation of the chaperone TRAP1. *Cell Rep* 18: 659−672

46. De Smet P, Parys JB, Callewaert G, Weidema AF, Hill E, De Smedt H, Erneux C, Sorrentino V, Missiaen L (1999) Xestospongin C is an equally potent inhibitor of the inositol 1,4,5-trisphosphate receptor and the endoplasmic-reticulum Ca(2+) pumps. *Cell Calcium* 26: 9−13